



# Modification of optical properties in ZnO particles by surface deposition and anchoring of NiO nanoparticles

F. Rubio-Marcos<sup>a,b,\*</sup>, C.V. Manzano<sup>c</sup>, J.J. Reinoso<sup>b</sup>, I. Lorite<sup>b</sup>, J.J. Romero<sup>b</sup>, J.F. Fernández<sup>b</sup>, M.S. Martín-González<sup>c</sup>

<sup>a</sup> Departamento de Física de Materiales, UCM, 28040 Madrid, Spain

<sup>b</sup> Instituto de Cerámica y Vidrio, CSIC, 28049 Madrid, Spain

<sup>c</sup> IMM-Instituto de Microelectrónica de Madrid (CNM-CSIC), Isaac Newton 8, PTM, E-28760 Tres Cantos, Madrid, Spain

## ARTICLE INFO

### Article history:

Received 12 August 2010

Received in revised form

15 November 2010

Accepted 22 November 2010

Available online 30 November 2010

### Keywords:

Zinc oxide

Nanoparticles

Surface

Photoluminescence

## ABSTRACT

Nanodispersion of NiO nanoparticles on the surface of ZnO microparticles has been carried out by means of a low energy dry mixing method. This method keeps the shape and size of the ZnO microparticles that served as support to hold the NiO nanoparticles. The dispersion and anchoring of the NiO nanoparticles takes place by means of an electrochemical reaction with the OH-groups present at the ZnO surface. The process took place at room temperature and cation interdiffusion between ZnO and NiO have not been detected by structural analysis. Nevertheless, changes in the optical properties of semiconductor ZnO particles have been observed due to the deposition of the nanoparticles. These changes correlate with the amount of NiO nanoparticles at the ZnO particle surface. The amount of defects, i.e. oxygen vacancies, interstitial oxygen and zinc vacancies, rises with the increasing NiO content.

© 2010 Elsevier B.V. All rights reserved.

## 1. Introduction

It has been observed that the interface created after a partial reaction of two oxides exhibits new and interesting properties due to the proximity and diffusion phenomena [1–4], which becomes relevant only at the nanoscale range. An interesting example of these interphase-related properties is the appearance of ferrimagnetism in mixtures of ZnO and Co<sub>3</sub>O<sub>4</sub>, despite the fact that they present diamagnetic and paramagnetic characteristics at room temperature, respectively [5,6]. The mixtures were prepared by a patented low energy dry mixing method [7] that produces a nanodispersion of Co<sub>3</sub>O<sub>4</sub> nanoparticles over ZnO microparticles. This nanodispersion is produced by mixing the appropriate quantities of microparticles and nanoparticles agglomerates for a defined time with a turbula mixer. Micro and nanoparticles move and crash freely inside a nylon container due to the absence of liquid media. The mechanical impacts produced between microparticles and the nanoparticles agglomerates break the latter, dispersing the nanoparticles. In some cases, a small amount of microballs are added to improve the dispersion process. The free nanoparticles show a very high reactivity and when colliding with the microparti-

cles they got stuck to their surfaces. This method has the advantages of being free from surfactants, avoiding changes of the particle surfaces, and not producing any change in the shape or size of the particles, due to the very low energy of the impacts. The patented method has been proved efficient in a high number of systems. This nanodispersion method has opened up a challenge to obtain nanoparticles interfaces with unusual properties by mixing oxides of dissimilar materials [8]. Moreover, this nanodispersion method will be very useful for anchoring nanoparticles on different types of substrates that present technological interest.

One of the candidates as micro-particles support is zinc oxide. ZnO is an important wurtzite-type semiconductor with band gap energy of 3.37 eV at room temperature and a very large exciton binding energy of about 60 meV. Moreover, it presents interesting chemical, acoustic, optical, and electrical properties [9,10].

On the other hand, NiO nanoparticles are commonly used for a wide range of applications. Nano-structured NiO is introduced as p-type semiconductor with a stable, wide band gap (3.6–4.0 eV) [11], although bulk NiO is an antiferromagnetic insulator with a Néel temperature ( $T_N$ ) of 523 K [12]. Important applications of nano-sized NiO include preparation of cathode materials for alkaline batteries [13], electrochemical capacitors [14], smart windows [15], active layers for gas sensors [16] and catalytic systems [17].

This paper will present and discuss the effects of NiO nanoparticles addition on the structural disorder of the ZnO surface. It is shown that ZnO interface properties are modified by the high

\* Corresponding author at: Instituto de Cerámica y Vidrio, CSIC, Departamento de Electrocerámica, Kelsen No. 5, 28049 Madrid, Spain.

E-mail address: [frmarcos@icv.csic.es](mailto:frmarcos@icv.csic.es) (F. Rubio-Marcos).

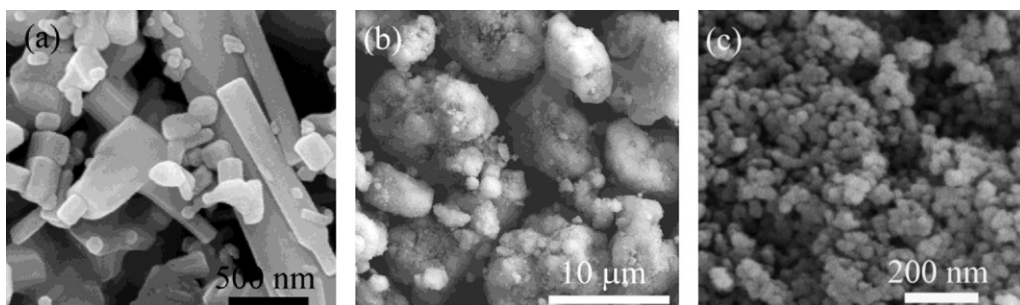


**Fig. 1.** Field emission-scanning electron microscopy micrograph of the initial materials: (a) ZnO microparticles, (b) NiO nanoparticles agglomerates and (c) detail of NiO spherical nanoparticles.

surface reactivity of the oxide nanoparticles producing changes in the optical and structural properties of the ZnO.

## 2. Experimental

**Nanodispersion procedure of ZnO/NiO mixtures:** Compositions with 1, 5 and 25 wt% of NiO nanoparticles (hereafter named as ZN1, ZN5 and ZN25, respectively) were prepared by incorporating the appropriate amounts of NiO nanoparticles to ZnO microparticles by a previously described dry solid state method, producing an electrochemical reaction at room temperature [7]. The dry dispersion process consisted on shaking the materials mixture in a 60 cm<sup>3</sup> nylon container for 5 min at 50 rpm using a turbula-type mixer. The process was aided by the addition of ZnO<sub>2</sub> balls with a diameter of 1 mm. Pure ZnO and NiO powders were also submitted independently to the same mixing process to ensure that no structural disorder was induced on any material by the mixing process. The raw materials used in this study were nickel oxide (NiO, 99.9%), and ZnO (>99.99%). Analytical grade powders were dried at 110 °C for 2 h before dry mixing.

**Morphology characterization:** The particle size and morphology of the powders were evaluated using secondary electron images of field emission scanning electron microscopy, FE-SEM (Hitachi S-4700) and transmission electron microscopy (TEM, Hitachi H-7100 175) with an accelerating voltage of 120 kV. For TEM investigations, powders were suspended in isopropanol, and a drop of this suspension was deposited on a holey carbon-coated film supported on a 400 mesh copper grid. The crystalline structure was determined by X-ray diffraction analysis (XRD, Siemens D5000, Munich, Germany, Cu K $\alpha$  radiation).

**Optical properties characterization:** The reflectivity of the sample was collected with a UV-NIR spectrometer equipped with an integration sphere (PerkinElmer 950). The UV-NIR spectra were measured at room temperature in the wavelength range of 300–800 nm. Raman spectra were measured in air atmosphere at room temperature, using 514 nm radiation from an Ar<sup>+</sup> laser operating at 10 mW. The signal was collected by a microscope Raman spectrometer (Renishaw Micro-Raman System 1000) in the 100–1100 cm<sup>-1</sup> range. For the photoluminescence (PL) characterization, the sample was optically pumped at 355 nm with a tripled Nd-YAG pulsed laser (pulse duration 15 ns and repetition rate 20 kHz). The spectra were recorded at room temperature using a monochromator and a photomultiplier tube.

## 3. Results and discussion

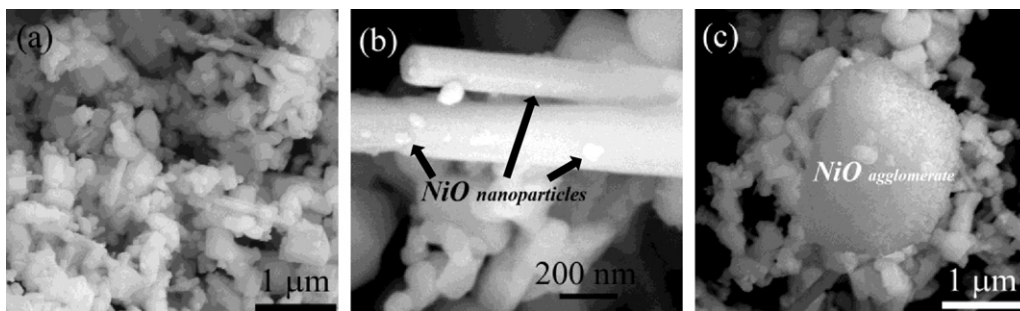
### 3.1. Morphology of the nanodispersed ZnO/NiO mixtures

Fig. 1 shows the morphology of pure ZnO and NiO before mixing. The FE-SEM micrograph (Fig. 1(a)) shows the typical ZnO morphol-

ogy consisting mainly on elongated prismatic particles and nearly cubical particles, with sizes of 0.5–1.0  $\mu$ m. The NiO nanoparticles present spherical shapes with diameters of 20–30 nm [see Fig. 1(c)]. These particles form globular agglomerates of  $\sim$ 5.0  $\mu$ m, as shown in Fig. 1(b).

The mixture of ZnO with 5 wt% of NiO nanoparticles is shown in Fig. 2(a). The micrographs show that most of the NiO agglomerates disappear and individual nanoparticles are adhered to the ZnO surface (Fig. 2(b)). The dispersion and great adherence of nanoparticles indicate that a spontaneous reaction occurs at room temperature between these materials, due to the high initial reactivity of the NiO and ZnO. This novel way to de-agglomerate nanoparticles has also been applied previously in other mixtures [7,18], producing novel properties at the interfaces. For NiO contents lower than 5 wt% all individual nanoparticles are completely dispersed over the surface of the ZnO particles, whereas for higher NiO contents nanoparticles agglomerates started to appear (Fig. 2(c)). This means that there is a “saturation amount” of NiO that can be effectively dispersed over ZnO microparticles before agglomerates are observed. This fact is correlated with the ZnO microparticles surface. It is worth mentioning that ZnO particles morphology is kept invariant, as a result of the low energy of the mixture process. So, no new ZnO surfaces are formed during the mixing process. It has been reported that an energetic milling provokes surface defects in ZnO [19]. For this reason, and for comparison purposes, we also performed the same low energy process in pure ZnO particles and NiO nanoparticles, observing no differences whatsoever on the particles morphology or properties.

The TEM micrograph in Fig. 3 confirms the formation of ZnO–NiO interfaces after the dry mixing process. It can be observed, from the inset of Fig. 3(a), that  $\sim$ 25 nm NiO nanoparticles are distributed on the surface of the ZnO particles (needle like in this case). For comparison purposes TEM of NiO nanoparticles after the same dry mixing process is observed in Fig. 3(b). These particles do not show any changes in shape or size due to the mixing process, and they present the same agglomeration state observed in non-milled pow-



**Fig. 2.** Field emission-scanning electron microscopy micrograph of ZnO particles covered by NiO nanoparticles adhered at the surface after low energy mixing. (a) Mixture of ZnO with 5 wt% of NiO nanoparticles, (b) detail of the NiO nanoparticles dispersed over ZnO elongated prismatic particles and (c) NiO agglomerates observed in the mixtures with NiO contents higher than 5 wt%.

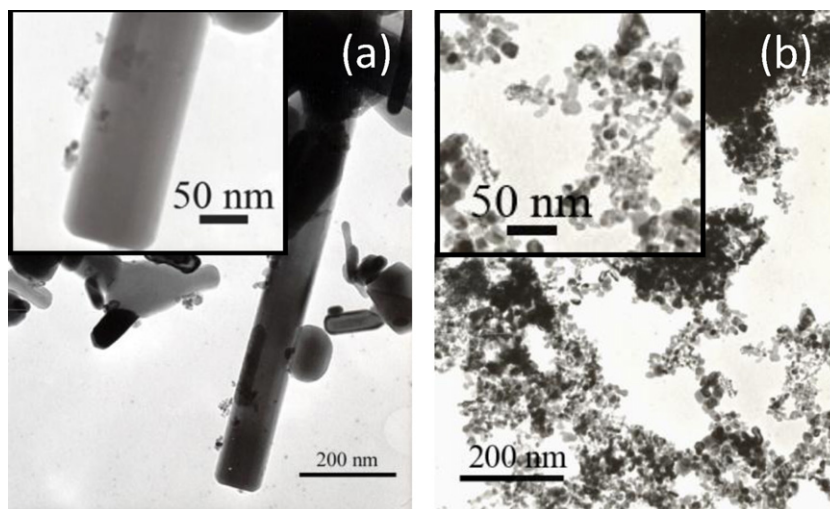


**Fig. 3.** (a) TEM micrograph of Zn5 mixture. The inset shows NiO nanoparticles adhered at the ZnO surface particles. (b) TEM micrograph of NiO nanoparticles. The inset shows individual NiO nanoparticles with a medium size diameter of  $\sim 25$  nm.

ders. Moreover, the interphases between both particles are clear and well defined, indicating that no interdiffusion or secondary phases appeared in the contact region. The X-ray diffraction pattern of the raw materials and the ZnO/NiO mixtures, displayed in Fig. 4, can be indexed on the basis of a phase mixture constituted by a majority of ZnO and a minority of NiO. Increasing the NiO amount implies that the minority phase increases, as expected. No variation on either ZnO or NiO lattice constant has been observed, demonstrating that the mixing method does not alter the particles; indicating that no doping processes take place between both materials. On the other hand, it is well known that X-ray diffraction (XRD) supplies average structural information. This means that if any local change occurs at the interfaces between NiO and ZnO, it could not be detected by this technique.

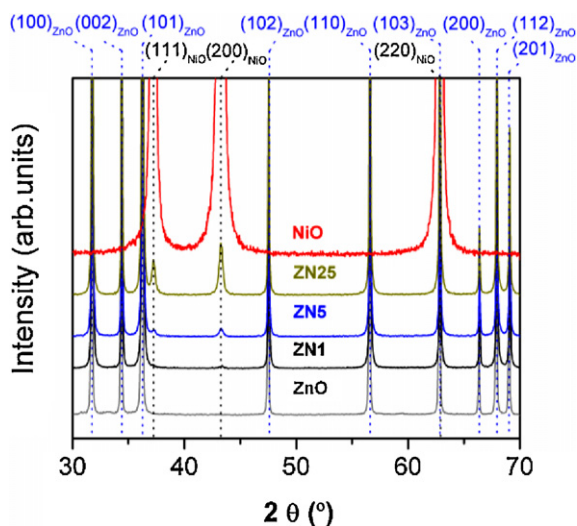
### 3.2. Nanodispersion evaluation by UV–vis absorption

Fig. 5 shows the diffuse reflectivity at the ZnO absorption edge as a function of the NiO content in the mixture. While ZnO particles are white, NiO nanoparticles are black, so the mixtures must acquire a grey colour, i.e. a reduction of the reflectance on the whole visible

region. However, this reduction does not present a linear dependence with the NiO addition to the mixtures. The reflectance loss is related to the effectiveness of the dispersion of NiO nanoparticles on the ZnO particles, since no new reflecting ZnO surfaces are formed during the mixing process. A rapid decrease of reflectance is observed for the samples with a concentration of NiO nanoparticles up to 5 wt% (where the FE-SEM images show full dispersion of the NiO nanoparticles on the ZnO surface). For higher NiO contents there is a change in the slope of the curve corresponding to a reduction of the reflectivity change rate. This is related to the presence of agglomerates, whose efficiency to cover the surface of the particles is lower than for the dispersed NiO nanoparticles. Therefore the dry method used here is effective for NiO contents up to 5 wt% and this fact is related to the presence of surface sites on the ZnO microparticles surface which can react with the NiO nanoparticles.

### 3.3. Optical characterization of ZnO/NiO mixtures

Fig. 6(a) shows the Raman spectra for the ZnO and the ZnO/NiO mixtures. ZnO has a wurtzite structure, with two formulae per primitive cell with  $C_{3v}$  symmetry. The Raman spectrum of ZnO powder submitted to the dispersion process, does not shown here for the sake of clarity, does not show any difference with the one of the original powder, indicating that the mixing process



**Fig. 4.** XRD patterns corresponding to the ZnO/NiO mixtures. The peaks can be indexed and labeled on the basis of the mixture of ZnO and NiO.

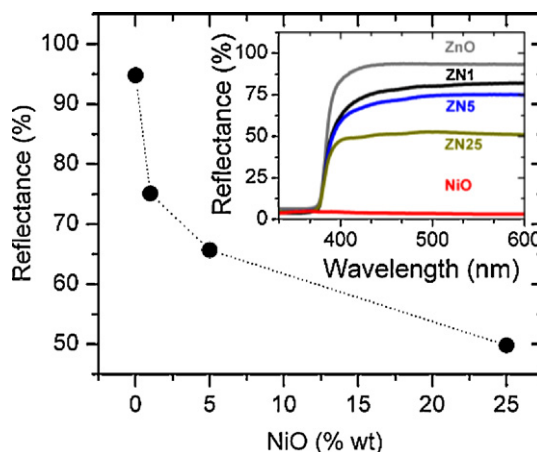


**Fig. 5.** Diffuse reflectivity at the ZnO absorption edge in function of NiO content in the mixture. The insert shows UV–NIR diffuse reflectivity of the different samples.



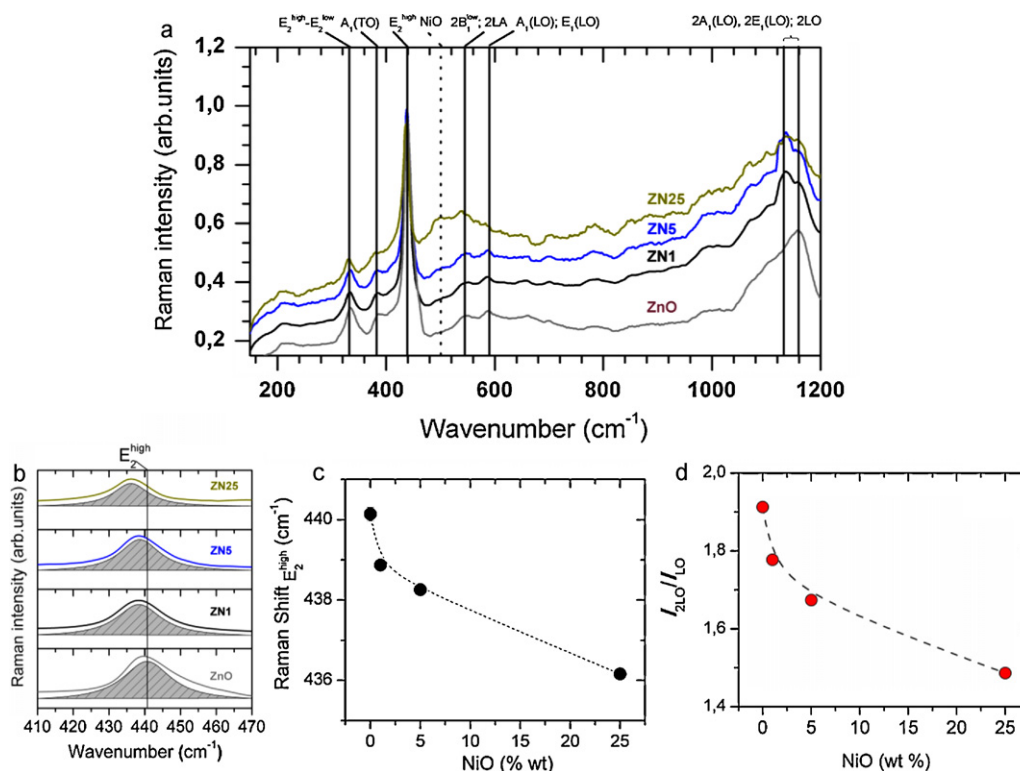


**Fig. 6.** (a) The Raman spectra of ZnO microparticles and ZnO/NiO mixtures as a function of the NiO content. (b) Magnified Raman spectra in the wavenumber ranges from 410 to 470  $\text{cm}^{-1}$  of the ZnO microparticles and ZnO/NiO mixtures and Lorentzian fits of the individual peak of the  $E_2^{high}$  Raman modes as a function of NiO content. (c) Evolution of the Raman shift of  $E_2^{high}$  Raman modes as a function of NiO content. (d) Variations of the intensity ratio of the second-order Raman mode (2LO) over the first-order (LO) mode,  $I_{2LO}/I_{LO}$ , as a function of the NiO content.

does not produce measurable effects on the ZnO particles. For this structure, the group theory predicts four Raman active modes,  $A_1 + E_1 + 2E_2$  [20]. It is obvious from Fig. 6(a) that NiO addition modifies Raman spectra, causing Raman intensity to decrease, as well as an energy shift and broadening of particular modes of ZnO. This must be related to some interaction between NiO and ZnO particles. The  $E_2^{high}$  mode, located at  $\sim 436 \text{ cm}^{-1}$  in the Raman spectrum of ZnO [20], goes through significant changes, as shown in Fig. 6(b), where the spectrum region between 410 and 470  $\text{cm}^{-1}$  is fitted to a Lorentzian function. This Raman mode, assigned to the oxygen vibrations [20], is very intense. Its pronounced asymmetry is attributed to lattice disorder, as well as to anharmonic phonon–phonon interactions [20]. The  $E_2^{high}$  mode of ZnO broadens and shows an intensity decrease and redshifting (up to 4  $\text{cm}^{-1}$ ) when NiO nanoparticles are bound to its surface (see Fig. 6(c)). These points out changes in the defect structure on the ZnO surface due to the adhesion of NiO nanoparticles. The non linear evolution of the Raman shift of  $E_2^{high}$  shown in this graph is correlated with the non linearity observed in the diffuse reflectivity of the mixtures and with the “saturation concentration” detected by FE-SEM. The fact that the  $E_2^{high}$  Raman mode, originated from the oxygen vibrations in the ZnO crystal lattice, is more affected by the NiO addition than the  $E_2^{low}$  mode, ascribed to the Zn sublattice vibrations [19], suggests that the oxygen defects probably dominate after NiO addition.

The NiO addition also induces significant changes in the position, full width at half maximum (FWHM) and intensity of the  $E_1(LO)$  and  $A_1(LO)$  Raman modes. It should be noticed that the  $A_1(LO)$  mode at  $\sim 569 \text{ cm}^{-1}$  and the  $E_1(LO)$  mode at  $\sim 586 \text{ cm}^{-1}$  have relatively close wavenumbers and rise from the background, which is originated from second-order Raman scattering. The presence of impurities and/or defects can influence both these modes. The  $E_1(LO)$  mode also slightly redshifts from  $\sim 587 \text{ cm}^{-1}$  in ZnO pow-

der up to  $\sim 584 \text{ cm}^{-1}$  in Zn5 sample. Since the ZnO  $E_1(LO)$  mode is related to oxygen vacancies, its intensity increases and redshift with NiO addition points out to serious oxygen deficiency in the mixed powders [19,21]. A shift to lower wavenumber indicates a structural relaxation of the crystalline lattice due to reduction of structural stress [22]. However, in our case, this shift is originated by the presence of NiO nanoparticles on the ZnO surface, since new ZnO surfaces are not formed by this process. In addition, the  $A_1(LO)$  Raman mode, that corresponds to local vibration modes associated with intrinsic lattice defects, may also be favored by the NiO nanoparticles proximity [23]. This mode is present only in Zn25 samples. The anomalous enhancement of the LO mode has also been reported in doped ZnO [24–26], and ascribed to oxygen vacancies and interstitial Zn.

On the other hand, the high-wavenumber region in the Raman spectra of ZnO is dominated by a broad asymmetric mode at  $\sim 1154 \text{ cm}^{-1}$ , containing contributions of  $2A_1(LO)$  and  $2E_1(LO)$  modes at the  $\Gamma$  point of the Brillouin zone [23]. The intensity decrease of the most intense second-order Raman mode with NiO addition is accompanied by a redshift (from  $\sim 1154 \text{ cm}^{-1}$  in ZnO down to  $\sim 1140 \text{ cm}^{-1}$  in Zn25) and broadening. The intensity ratio of this mode to the first-order  $E_1(LO)$  mode,  $I_{2LO}/I_{LO}$ , in ZnO and Zn samples can be used to estimate the electron–LO phonon coupling strength [27,28]. The  $I_{2LO}/I_{LO}$  ratio is decreasing with NiO amount from  $\sim 1.92$  in ZnO down to  $\sim 1.48$  in Zn25 (Fig. 6(d)). This behavior has been observed previously in mechanically activated ZnO [19]. Moreover, a clear splitting of  $2A_1(LO)$  and  $2E_1(LO)$  modes can also be observed with increasing NiO addition.

These results indicate that the electron transition of the ZnO structure can be modified through mixing NiO nanoparticles with ZnO powders to generate nanoparticle–microparticle interfaces. The above relations show that there is a correlation between the Raman shift and the NiO content, the non linearity of this cor-

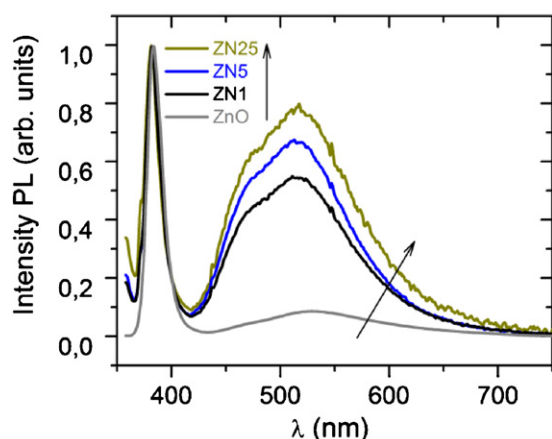


**Fig. 7.** PL spectra from the ZnO/NiO mixtures at 300 K upon excitation with 355 nm light.

relation being due to the non linear dispersion efficiency of the nanoparticles and the fact that a saturation concentration of NiO particles on ZnO surface exists. Nonetheless, it is not possible to explain the origin and nature of the defects on ZnO structure only by Raman spectroscopy.

To shine some light on the possible origin of these defects, photoluminescence (PL) studies were performed. Fig. 7 shows the PL spectra of pure ZnO submitted to the mixing process (no luminescence response can be observed on pure NiO with the current

experimental setup). The emission of pure ZnO is dominated by near-band-edge (NBE) UV emission with a maximum at 382 nm (3.25 eV), which corresponds with the band gap of ZnO. In the visible range, weaker emission bands between 420 and 650 nm can be observed. These bands must be associated to defects and/or impurities. The emission at 420–650 nm is too wide to be associated to only one defect or impurity, so it should be deconvoluted into three bands: a blue component centered at 465 nm (2.67 eV), a green one at 515 nm (2.41 eV) and a yellow one at 550 nm (2.25 eV), which could be assigned to interstitial oxygen [29]. The blue emission can be associated with a transition from oxygen vacancies energy states to valence band and the green emission is associated with zinc vacancies [30]. The strong UV emission intensity in relation to the weak visible bands indicates that the ZnO particles are nearly free from defects. The mixing process at low energy used in this work prevents the formation of new ZnO surfaces and, consequently, the appearance of surface defects. After mixing ZnO particles with different amounts of NiO (Fig. 7) an important increase in the intensity of the visible bands is detected (after spectra are normalized to the 382 nm band). This means that the number of defects (oxygen vacancies and zinc vacancies) increases with the NiO nanoparticles addition. The analysis of the bands in the visible region is presented in Fig. 8(a) and (b). A detail of this region is presented in Fig. 8(a), where the spectrum is fitted to the sum of three Lorentzian functions centered at ~465 nm, ~515 nm and ~550 nm and ascribed to oxygen vacancies ( $V_O$ ), zinc vacancies ( $V_{Zn}$ ) and interstitial oxygen ( $O_i$ ), respectively [29,30]. The area of the bands in the visible region between 420 and 650 nm as a function of the NiO concentration shows, again, a non-linear trend with the NiO concentration

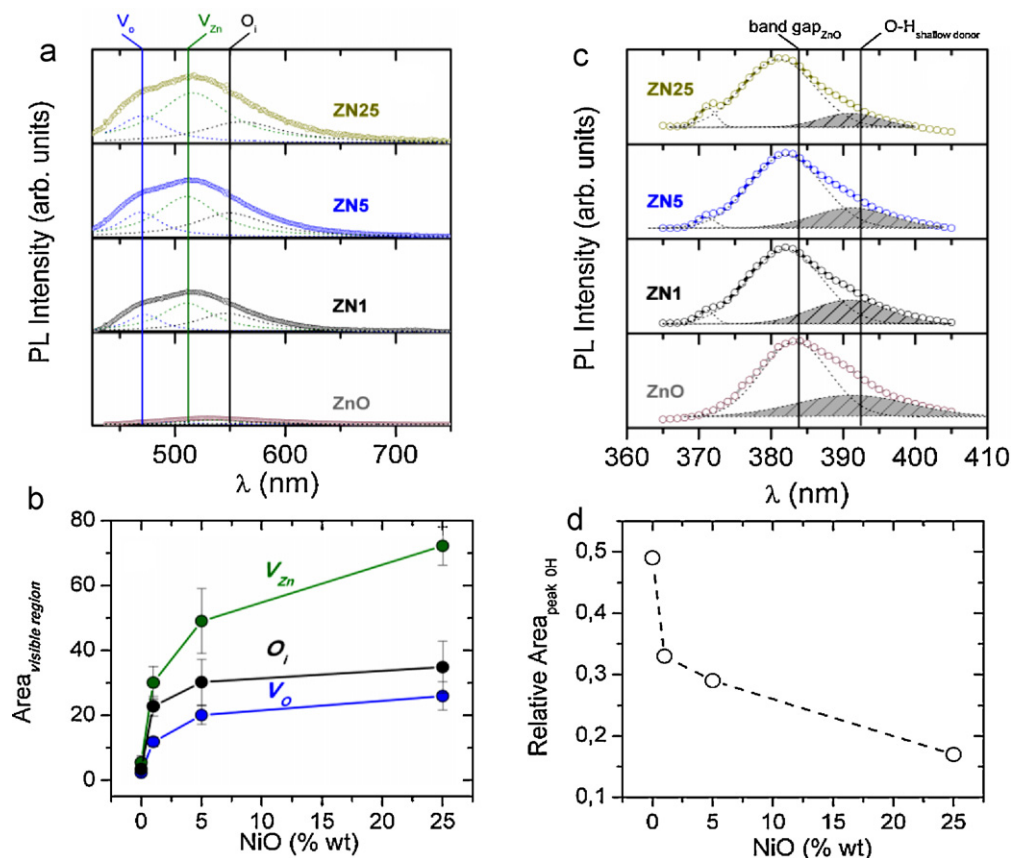


**Fig. 8.** (a) Magnified PL spectra in the wavelength ranges from 425 to 750 nm of the ZnO microparticles and ZnO/NiO mixtures as a function of NiO content. In the same figure, Lorentzian fits of the individual bands centered at ~465 nm, ~515 nm and ~550 nm, and ascribed to oxygen vacancies ( $V_O$ ), zinc vacancies ( $V_{Zn}$ ) and interstitial oxygen ( $O_i$ ). (b) Area evolution of the bands in the visible region between 420 and 650 nm as a function of the NiO concentration. (c) Magnified PL spectra in the near-band-edge (NBE) UV and Lorentzian fit of the individual band ascribed to hydrogen of the OH group which behaves as a shallow donor in ZnO of the different samples and (d) relative area [ $area_{3.17\text{eV}}/area_{3.25\text{eV}}$ ] in function of the NiO concentration.

(Fig. 8(b)). Then, it can be concluded that the quantity of defects, i.e. oxygen vacancies, interstitial oxygen and zinc vacancies rises upon increasing the NiO concentration in the mixture, with the same nonlinear tendency observed previously in this study.

It is very important to note here that the NBE emission also changes with the concentration of NiO in the mixture (Fig. 8(c)). The main emission band is displaced from 3.23 eV for pure ZnO to 3.25 eV for the sample with a 25 wt% in NiO. This change could be related to the stress relaxation of the crystalline lattice determined by the Raman shift of the  $E_1(\text{LO})$  mode related to oxygen vacancies. In addition, there is also another emission band that appears at 3.17 eV. This band has been assigned to hydrogen of the OH group which behaves as a shallow donor in ZnO with an activation energy of 53 meV [31,32]. Regarding this emission, an interesting change is observed. Its relative area [ $\text{area}_{3.17\text{eV}}/\text{area}_{3.25\text{eV}}$ ] is reduced by increasing the concentration of NiO in the mixture, see Fig. 8(d). This reduction shows the same non-linear behavior with the NiO content previously observed for the reflectance and the Raman shift. This result indicates that the content of OH groups located at the ZnO surface diminished by the presence of NiO nanoparticles. The presence of hydroxyl groups is commonly observed in oxide surfaces exposed to atmospheric conditions. The elimination of surface OH-groups with the NiO addition implies that a solid state reaction occurs at the ZnO–NiO interface [18]. This reaction takes place at the surface of the ZnO when mixed with NiO and can be understood in terms of the high reactivity of the oxides surface. This phenomenon produces a modification on the ZnO particle surface and could explain the increase in  $V_{\text{O}}$ ,  $V_{\text{Zn}}$  and  $\text{O}_i$  detected by PL.

We reported previously the appearance of such a reaction in ZnO–Co<sub>3</sub>O<sub>4</sub> mixtures produced by the dry dispersion method in which nanoparticles are effectively dispersed onto microparticles [8,18]. The non-linear relationship observed between the different optical parameters and the NiO quantity can be related to the maximum number of OH groups present on the surface of the ZnO particles. When the amount of nanoparticles is low, most of them can find a surface OH group and the reaction takes place. When the NiO concentration is too high, no active OH groups are available and the nanoparticles do not desagglomerate anymore.

#### 4. Conclusions

In summary, we demonstrated a novel method to disperse NiO nanoparticles on ZnO surface. This dispersion modifies optical properties of the ZnO by a solid state electrochemical reaction at the ZnO–NiO interface mediated by surface OH groups. This reaction produced a stress relaxation of the ZnO surface and the introduction of some structural disorder. These modifications on the ZnO are translated to changes in emission properties. The implications of the present findings introduce tools to modify optical properties of semiconductors by the use of nanoparticles adequately dispersed on the surface of microparticles.

#### Acknowledgments

The authors express their thanks to the CICYT project MAT2010-21088-C03-01, MAT2008-06330, PLE2009-0073, and to the European Commission ERC-2008-Stg: 240497 for their financial support. MSMG want to acknowledge B. Alen from IMM for technical support.

#### References

- [1] A. Brinkman, M. Huijben, M. Van Zalk, J. Huijben, U. Zeitler, J.C. Maan, W.G. Van der Wiel, G. Rijnders, D.H.A. Blank, H. Hilgenkamp, *Nat. Mater.* 6 (2007) 493.
- [2] F.Y. Bruno, J. Garcia-Barriocal, M. Torija, A. Rivera, Z. Sefrioui, C. Leighton, C. Leon, J. Santamaria, *Appl. Phys. Lett.* 92 (2008) 082106.
- [3] R.K. Singhal, M.S. Dhawana, S.K. Gaura, S.N. Doliaa, S. Kumarb, T. Shripathic, U.P. Deshpandec, Y.T. Xingd, E. Saitovitchd, K.B. Garga, *J. Alloys Compd.* 477 (2009) 379.
- [4] A. Singhal, *J. Alloys Compd.* 507 (2010) 312.
- [5] A. Quesada, M.A. García, M. Andrés, A. Hernando, J.F. Fernández, A.C. Caballero, M.S. Martín-González, F. Briones, *J. Appl. Phys.* 100 (2006) 113909.
- [6] M.S. Martín-González, J.F. Fernández, F. Rubio-Marcos, I. Lorite, J.L. Costa-Krämer, A. Quesada, M.A. Bañares, J.L.G. Fierro, *J. Appl. Phys.* 103 (2008) 083905.
- [7] J.F. Fernández, I. Lorite, F. Rubio-Marcos, J.J. Romero, M.A. García, A. Quesada, M.S. Martín-González, J.L. Costa-Krämer, Patent Number: WO2010010220-A1 (2010).
- [8] F. Rubio-Marcos, V. Calvino, M.A. Bañares, J.F. Fernández, *J. Catal.* 275 (2010) 288.
- [9] F.C.M. Van De Pol, *Am. Ceram. Soc. Bull.* 69 (1990) 1959.
- [10] C.F. Kilingshrim, *Semiconductor Optics*, Springer, Berlin, 1995, p. 309.
- [11] H. Yang, Q. Tao, X. Zhang, A. Tang, J. Ouyang, *J. Alloys Compd.* 459 (2008) 98.
- [12] C.D. Guerra, A. Remón, J.A. García, J. Piqueras, *Phys. Status Solidi A–Appl. Mater.* 163 (1997) 497.
- [13] J. Bahadur, D. Sen, S. Mazumder, S. Ramanathan, *J. Solid State Chem.* 181 (2008) 1227.
- [14] T. Nathan, A. Aziz, A.F. Noor, S.R.S. Prabakaran, *J. Solid State Electrochem.* 12 (2008) 1003.
- [15] C.G. Granqvist, *Handbook of Inorganic Electrochromic Materials*, Elsevier, Amsterdam, 1995.
- [16] I. Hotovy, J. Huran, L. Spiess, S. Hascik, V. Rehacek, *Sens. Actuator B–Chem.* 57 (1999) 147.
- [17] S.-M. Tana, S.-P. Chaia, W.-W. Liuc, A.R. Mohameda, *J. Alloys Compd.* 477 (2009) 785.
- [18] M.S. Martín-González, M.A. García, I. Lorite, J.L. Costa-Krämer, F. Rubio-Marcos, N. Carmona, J.F. Fernández, *J. Electrochem. Soc.* 157 (2010) E31.
- [19] M. Šćepanović, M. Grujić-Brojčin, K. Vojisavljević, S. Bernik, T. Srečković, 41, *J. Raman Spectrosc.* (2010) 914.
- [20] C.A. Arguello, D.L. Rousseau, S.P.S. Porto, *Phys. Rev.* 181 (1969) 1351.
- [21] F. Rubio-Marcos, A. Quesada, M.A. García, M.A. Bañares, J.L. García Fierro, M.S. Martín-Gonzalez, J.L. Costa-Krämer, J.F. Fernández, *J. Solid State Chem.* 182 (2009) 1211.
- [22] G. Gouadec, P. Colombar, *Prog. Cryst. Growth Charact. Mater.* 53 (2007) 1.
- [23] R. Cuscó, E. Alarcón-Lladó, J. Ibáñez, L. Artús, J. Jiménez, B. Wang, M.J. Callahan, *Phys. Rev. B* 75 (2007) 165202.
- [24] J.M. Liu, C.K. Ong, L.C. Lim, *Ferroelectrics* 231 (1999) 223.
- [25] S.K. Sharma, G.J. Exarhos, *Solid State Phenom.* 55 (1997) 32.
- [26] C.L. Du, Z.B. Gu, M.H. Lu, J. Wang, S.T. Zang, J. Zhao, G.X. Cheng, H. Heng, Y.F. Chen, *J. Appl. Phys.* 99 (2006) 123515.
- [27] M. Šćepanović, T. Srečković, M.K. Vojisavljević, M.M. Ristić, *Sci. Sintering* 38 (2006) 169.
- [28] R.P. Wang, G. Xu, P. Jin, *Phys. Rev. B* 69 (2004) 113303.
- [29] M. Liu, A.H. Kitai, P. Mascher, *J. Lumin.* 54 (1992) 35.
- [30] A. Janotti, C.G. Van de Walle, *Phys. Rev. B* 76 (2007) 165202.
- [31] E.V. Lavrov, F. Börrnert, J. Weber, *Phys. Rev. B* 72 (2008) 085212.
- [32] E.V. Lavrov, F. Herklotz, J. Weber, *Phys. Rev. Lett.* 102 (2009) 185502.